Inorganic Chemistry

Article

pubs.acs.org/IC

New Insights on the Incorporation of Lanthanide Ions into Nanosized Layered Double Hydroxides

Tamara Posati,[†] Ferdinando Costantino, Loredana Latterini, Morena Nocchetti,* Marco Paolantoni, and Luigi Tarpani

Dipartimento di Chimica and Centro di Eccellenza Materiali Innovativi Nanostrutturati (CEMIN), Università di Perugia, Via Elce di Sotto, 8, 06123 Perugia, Italy

Supporting Information

ABSTRACT: Nanosized Layered Double Hydroxides (LDH) were prepared in confined environment through the microemulsion method in the presence of different lanthanide cations (Ln(III) = Eu(III), Yb(III), Tb(III), and Nd(III)). To investigate the effects of lanthanide insertion in the sheets of LDH materials, several samples were prepared upon progressively increasing the content of Ln ions and properly reducing the Al(III) amount; the samples were characterized in terms of metal content, structure, morphology, thermal behavior, and spectroscopic properties. The data revealed that Ln(III) content in the LDH samples depends on the ionic radius of the lanthanide cations and on its concentration in the starting microemulsion. X-ray powder diffraction (XRPD) indicated that Eu(III) can be inserted into the LDH structure in average atomic percentages lower than 2.7%, leading to the formation of a low symmetry phase, as confirmed by steady state luminescence spectra; while Yb(III) can be incorporated into the layer structure up to about 10% forming a pure layered phase containing the lanthanide in the sheet. The incorporation of Yb(III) and Eu(III) into the LDH sheets is also supported by FT-IR measurements. Coupled thermogravimetrical (TG) and differential scanning calorimetric (DSC) studies indicated that water molecules are essential in the coordination sphere of incorporated Ln cations; this observation accounts for the lower thermal stability of Ln-doped LDH compared to the undoped ones. Furthermore, Eu-luminescence measurements indicates that the lanthanide inclusion does not compromise its luminescence although the spectral position and brightness can be tuned by the loading.

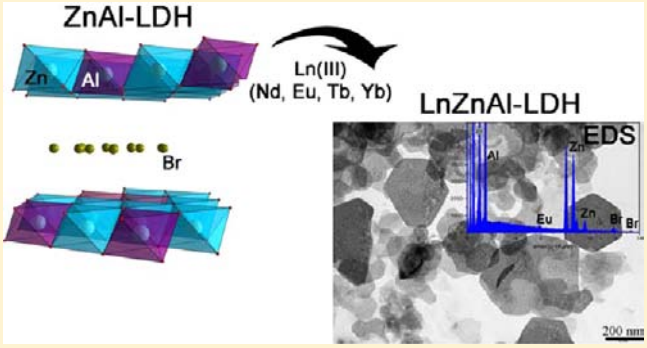

INTRODUCTION

The synthesis of inorganic layered compounds possessing good intercalation properties to be used for the design of new host–guest systems is a research topic of wide interest. These compounds can find application in many fields involving the development of new functional materials ranging from materials for energy conversion and storage to biomedical compounds. A recent and promising feature concerns the attainment of layered hydroxides containing lanthanide ions to combine the optical, magnetic, and catalytic properties of lanthanides with the flexibility of layered hosts.

A family of well established layered materials are the Layered Double Hydroxides (LDH)[1] represented by the general formula $[M(II)_{1-x}M(III)_x(OH)_2][A_{x/n}]\cdot mH_2O$, where M(III) cations are typically Al, Cr, Fe, Ga, M(II) are Mg, Zn, Ni, Co, Cu, and A^{n-} is a charge balancing anion with n as ionic valence; x represents the M(III) molar fraction referred to metals, and it is generally found between 0.20 and 0.40. These materials are also known as Hydrotalcite-like compounds (HTlc) for their structural analogies with the mineral Hydrotalcite, containing Mg(II) and Al(III) in a 3/1 molar ratio. Moreover, the inorganic hydroxide layer of a LDH is also called "brucitic sheet" because it is related to the layered mineral "brucite" of formula $Mg(OH)_2$. These layered compounds show excellent properties in terms of intercalation versatility toward a high number of inorganic and organic anions, good stability, easy and cheap synthetic preparation and low toxicity,[1−5] and they can be tested for different applications such as fillers for nanocomposites, drug-carriers, catalysts precursors, ordered thin film components and sensors, as suggested by the recent literature.[6−14] Several studies describe the intercalation and the luminescence properties of lanthanide anionic complexes into the LDH,[12,13] but their presence may hinder the accessibility of the interlayer region to other guest species. In this respect, the possibility to incorporate lanthanide cations (Ln(III)) directly into LDH sheets to obtain luminescent materials without filling the interlayer region is challenging for biomedical applications or for the development of new optoelectronic materials. One possible strategy to reach Ln(III) inclusion is to replace the M(III) cations present in the brucitic sheet, at least partially, by Ln(III) cations.

Received: July 20, 2012
Published: November 27, 2012

Lanthanide ions (Ln(III)) have ionic radii in the range from 0.85 to 1.04 Å and a coordination number ranging from 7 to 10 which is very different in comparison with that for the Al(III) ion (0.53 Å for a coordination number of 6); thus, an isomorphic substitution of Al(III) with Ln(III) could not generally be favorable without inducing detectable changes to the brucitic layer structure, having an octahedral coordination. These reasons allow to suppose that the rare-earth ions can be incorporated in the hydroxide brucitic layer only in small amounts, very likely by introducing distortions of the lattice as point defects.

Many attempts to directly synthesize LDHs containing lanthanide ions have been carried out in the recent past. However, clear experimental evidence on the coordination number of the lanthanide ions incorporated into LDH are still lacking. Stumpf et al.[15] reported that, in the Eu(III) doped MgAl-Cl-LDH, the Eu(III) ions are for the most part incorporated into the brucitic structure, whereas a minor part of them are inner-sphere adsorbed onto the LDH surface. Other authors suggested that Tb(III) and Eu(III) ions can be homogeneously incorporated in the lattice of LDHs with octahedral coordination.[16−23] Recently, Zhao et al.[24] synthesized MgAlEu-LDHs and, for the first time, reported that the Eu(III) ions can be incorporated into the LDH layer with a high coordination number (probably 8-coordinate). The europium incorporation led to a basal spacing increase, microstrain formation, and crystalline morphology imperfections. The existence of microstrain in the MgAlEu-LDHs structure generates broad diffraction peaks, and this is caused by vacancies or site disorder, plastic deformations in the LDH layers as a result of Eu(III) entering into the layers. To clarify some crucial aspects like the location and the environment of Ln(III) in a LDH, further detailed and methodical investigations must be performed. In a recent paper we have reported the synthesis and characterization of new nanosized LDHs containing Zn(II) and Al(III) as bivalent and trivalent metals respectively (hereafter called ZnAl LDH) and doped with Eu(III).[25] These materials have been obtained as nanoparticles through the synthetic method of the two microemulsions.[26,27] We have demonstrated that Ln ions can be incorporated in the LDH structures only when the materials are prepared as nanoparticles in a confined environment. In this connection a systematic approach to obtain new insights on the lanthanides incorporation on LDH has been here developed.

The aim of the present work is to investigate how the inclusions of Ln(III) ions with different ionic radius into nanosized ZnAl LDH affects the structure, the morphology, and the stability of the LDH. For this purpose, ZnAl LDH nanocrystals, doped with Ln(III), were prepared progressively substituting the Al(III) cation with increasing percentages of Ln(III). The structural changes of the LDH induced by different Ln(III) types and content have been studied by combining structural and spectroscopic techniques.

EXPERIMENTAL SECTION

Chemicals. Cetyltrimethylammonium bromide (CTABr), $Eu(NO_3)_3{\cdot}5H_2O$, $Yb(NO_3)_3{\cdot}5H_2O$, $Nd(NO_3)_3{\cdot}5H_2O$, and $Tb(NO_3)_3{\cdot}5H_2O$ were supplied by Aldrich. All other reagents were C. Erba RP-ACS products.

Synthesis of Ln-ZnAl LDH Nanoparticles in Microemulsion. Cetyltrimethylammonium bromide as surfactant, *n*-butanol as cosurfactant, and isooctane as the oil phase were used to prepare the microemulsions. Two microemulsions, designated A and B, with identical composition (in terms of CTABr, *n*-butanol, isooctane, and water), were prepared by dissolving different reagents in their aqueous phase. The aqueous phase of A was constituted of a 0.525 M salts solution (the amount of the used salts is shown in Supporting Information, Table SI-1), while the aqueous phase of B was a 1.25 M NH_3 solution. Microemulsions A and B were prepared by dispersing 6.25 g of CTABr and 7.75 mL of *n*-butanol in 18 mL of isooctane and then adding to each of these mixtures 6.75 mL of aqueous phase. The double-microemulsion processing route was then carried out by mixing equal volumes of the two initial microemulsions A and B to obtain the precipitation of LDH in the reverse micelles. The resulting system was stirred at room temperature for 15 min. After this time the system containing Eu, Nd, and Tb became cloudy whereas the one containing Yb became milk-like suggesting the formation of a precipitate. The systems were aged at 75 °C for 15 h. After aging, the particles were recovered by centrifuging (12000 rpm for 10 min), and a solid was obtained. The solid was washed with water (2 × 30 mL), and with a methanol-chloroform mixture (1:1) (2 × 30 mL) and then dispersed in water or dried at 60 °C under oil pump vacuum to give a fine powder. For the reader's convenience the samples Ln-ZnAl LDH, with Ln = Eu, Yb, Nd, Tb, will be labeled **1a−e**, **2a−d**, **3**, and **4** respectively (as indicated in the Supporting Information, Table SI-1).

Instrumental Procedures. The samples were characterized by chemical analysis, X-ray powder diffraction (XRPD), and thermal analysis. XRPD patterns were taken with a Philips X'PERT PRO MPD diffractometer operating at 40 kV and 40 mA, with a step size 0.0170 2θ degree, and step scan 20 s, using Cu Kα radiation and an X'Celerator detector.

Thermogravimetric (TG) analyses were performed with a Netzsch STA 449C apparatus, in air flow and with a heating rate of 10 °C/min. Differential scanning calorimetric (DSC) analyses were performed with a DSC 1 STAR System Mettler Toledo in air flow and with a heating rate of 10 °C/min.

Metal analyses were performed with Varian 700-ES series inductively coupled plasma-optical emission spectrometers (ICP-OES) using solutions prepared by dissolving the samples in concentrated HNO_3 and properly diluted. The carbon and hydrogen content was determined by elemental analysis using EA 1108 CHN FISONS instruments. To determine the Br^- counterion content, a given amount of sample (≈ 10 mg) was equilibrated in a Na_2CO_3 solution (10 mL, 0.5 M) for 12 h. The solution was then analyzed for the Br^- content with a Dionex 2000 Ion chromatograph equipped with an ionic conductivity detector.

The morphology of the samples was investigated with a Philips 208 transmission electron microscope (TEM) and with a FEG LEO 1525, scanning electron microscope. Energy dispersive spectroscopic analyses (EDS) and selected-area electron diffraction pattern (SAED) have been recorded using a Jeol 2010 operating at 200 kV and having a theoretical point-to-point resolution of 1.9 Å. The EDS spectrometer was equipped with an ultrathin window, capable of detecting elements heavier than boron. For the TEM images a small drop of the aqueous dispersion was deposited on a copper grid precoated with a Formvar film and then evaporated in air at room temperature.

The elemental mapping of metals in LDH samples was conducted by using energy dispersive X-ray spectroscopy (EDS) supported by a field emission scanning electron microscope (FE-SEM) (FEG LEO 1525). FE-SEM micrographs were collected after depositing the samples on a stub and sputter coating with chromium for 20 s.

A fluorimeter (Spex Fluorolog) equipped with a phosphorimeter (1934D) was used to record corrected luminescence spectra of the samples using the front face configuration between the excitation and the emission light for the powder samples.

Fourier-transform infrared spectra (FTIR) of different samples, dispersed in KBr pellets, were recorded using a Bruker Tensor 27 spectrometer. Typically each spectrum was obtained averaging over 50 scans at a resolution of 2 cm^{-1}.

RESULTS AND DISCUSSION

Sample Preparation and XRPD Measurement. Several samples of Ln-ZnAl LDH, with Ln = Eu (**1**), Yb (**2**), Nd (**3**), and Tb (**4**), have been prepared by the two microemulsions method[25] using different atomic percentages of the cations in the aqueous phase (phase A, see Experimental Section). The percentages of Zn(II), Al(III), and Ln(III), related to the total amount of metal ions, in the mother solution and in the obtained LDH-solid are reported in Table 1. The data show that the Ln(III) content in the solid can be changed by adjusting the amount of Ln(III) in the mother solutions.

Table 1. Molar Composition Percentages of the Metals in the Mother Solutions and in the Obtained Solids[a]

	solution (molar composition %) (±0.2%)			solid (molar composition %) (±0.3%)			
sample	Zn	Al	Ln	Zn	Al	Ln	*d* (Å)
1a	76.2	22.8	1	71.8	27.7	0.5	7.9
1b	76.2	21.8	2	73.1	26.0	0.9	8.0
1c	76.2	19.8	4	73.6	23.7	2.7	8.1
1d	76.2	18.8	5	72.9	23.0	4.1	7.9
1e	76.2	17.8	6	73.5	21.1	5.4	7.9
2a	76.2	21.8	2	73.8	24.7	1.4	7.9
2b	76.2	17.8	6	74.0	21.0	5	8.1
2c	76.2	13.8	10	76.4	16.1	7.4	8.6
2d	76.2	8.8	15	79.5	10.9	9.6	8.7
2e	76.2	3.8	20	81.4	1.6	17.0	9.7
3	76.2	21.8	2	75.4	24.1	0.5	7.9
4	76.2	21.8	2	72.6	27.4	1.2	7.9

[a]The interlayer distance (*d*) of the samples is also reported.

When the composition of the solutions with those of the corresponding solids are compared, a general trend can be observed: in the solid the aluminum molar percentage increases in spite of that of zinc and Ln(III). Note that the Ln(III) content in the solids, obtained from solutions having Ln(III) atomic percentage of 2 (samples **1b**, **2a**, **3**, **4**), decreases with the increase of the ionic radius. In addition, the europium amount in the samples **1a**−**1c** ranges from 45% to 67% of the content in the starting solution while the uptake of the smaller Yb ranges from 65% to 83% in the samples **2a**−**2d**; only the samples without phase segregation as europium hydroxides or zinc oxides have been considered (see discussion about XRPD measurement reported below). This finding suggests that there is a correlation between the Ln dimension and their uptake in the brucitic sheets, in particular the content of incorporated Ln(III) seems to decrease as the Ln(III) ionic radius increased.

Figure 1 shows XRPD patterns of **1b**, **2a**, **3**, and **4** samples in comparison with those of undoped ZnAl LDH sample. As observed in a previous paper,[25] in all the investigated samples the Ln doping of the brucitic sheet has the effect of generating small additional reflections in the XRPD patterns, indicated with and asterisk (*), that have been attributed to the formation of a low-symmetry phase, with monoclinic structure.[25] These reflections indicate the inclusion of Ln(III) in the LDH layer.

To investigate the maximum loading of Ln(III) ions included in the brucitic sheets, solid samples with increasing amount of

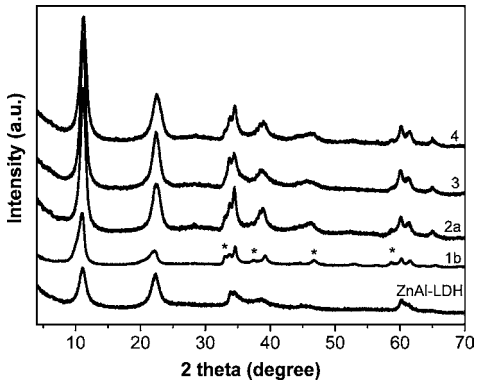

Figure 1. XRPD patterns of **1b**, **2a**, **3**, and **4** samples compared with undoped ZnAl LDH. (*) Reflections due to the monoclinic structure.

Eu and Yb, selected as representative of Ln ions with large and small ion radius respectively, have been prepared (Table 1). In Figures 2(A) and (B) the XRPD patterns of the **1a**−**1e** and **2a**−**2e** samples are compared. In samples **1**, the intensities of the additional reflections increase proportionally with the Eu amount (see samples **1a**, **1b**, and **1c** containing 0.5, 0.9, and 2.7% of Eu, respectively) and a small but progressive shift of the first basal reflections toward higher *d*-spacing values (from 7.9 to 8.1) is observed. Further increase of the Eu content leads to the appearance of sharp reflections in the 25−40° 2θ region that can be attributed to the formation of Eu(III) hydroxide (patterns **d** and **e**), at the same time the basal reflection shifts back to 7.9 Å, that is, the value of the undoped ZnAl LDH. In the diffraction patterns of the samples **2b**, **2c**, and **2d** some of the additional reflections increase in intensity whereas others disappear. Differently to **1**, the Yb amount included in the LDH solid can reach the 10% content, above which the formation of ZnO is observed (sample **2e**, Yb content 17%). In the sample **2d**, containing 9.6 atomic percentage of Yb, the reflections assigned to the undoped ZnAl LDH phase seem to disappear although the broadening of the reflections do not allow them to be successfully separated. Very likely, sample **2d** corresponds to a single phase containing Yb in the sheet. The cell parameters for the latter phase have been deduced by fitting the diffraction pattern with the LeBail method[28] (see Supporting Information, Figure SI-1) and, on the basis of our previous work on Eu-doped LDH,[25] a monoclinic cell with the following parameters has been found: a = 3.1155(8) Å, b = 5.474(1) Å, c = 16.83(2) Å, β = 94.8(8)°. This cell is very similar to that containing Eu, and the high values of the standard deviation of the cell parameters are due to the very large peak broadening. However, the similarities among them suggest that both Yb and Eu give similar structures and that the amount of the incorporated Ln ions into the sheet is due mainly to their size.

Despite the experimental evidence for a symmetry reduction (from hexagonal to monoclinic) due to the lanthanide insertion, a reliable structural model has not been found yet because the size of the particles and therefore the low quality of the diffraction patterns preclude any structure solution attempt. However, it is important to note that the first basal reflection of materials consistent with Ln(III) inclusion, tends to shift toward higher *d*-spacing values. Samples **2a**−**d** show an increase of *d* spacing from 7.9 to 8.7 Å with the Yb content. As a matter of fact a correlation between the increase of Yb atomic percentage and of the *d*-spacing value of the (002) reflection can be observed (Figure 3). As the bromide and the water

dx.doi.org/10.1021/ic301584g | Inorg. Chem. 2012, 51, 13229−13236

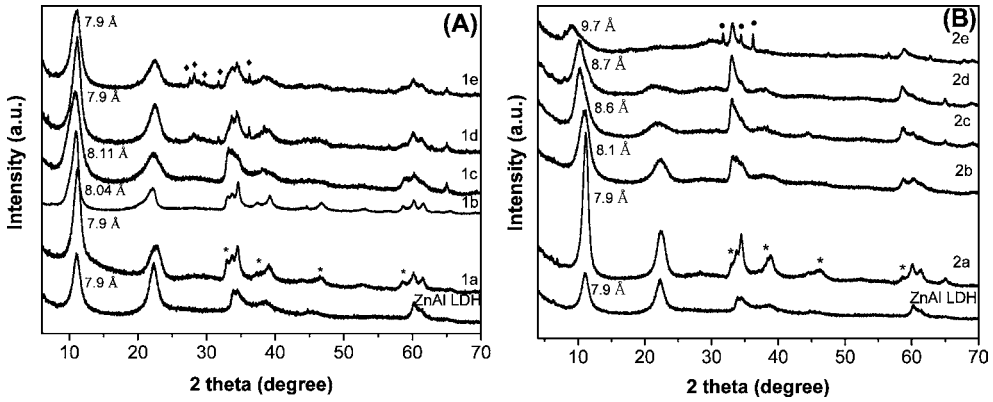

Figure 2. XRPD patterns of Eu-ZnAl LDH (**1a**−**1e**) (A) and of Yb-ZnAl LDH (**2a**−**2e**) (B) compared with undoped ZnAl LDH. (*) Reflections due to the monoclinic structure. $Eu(OH)_3$ (♦) and ZnO phases (●).

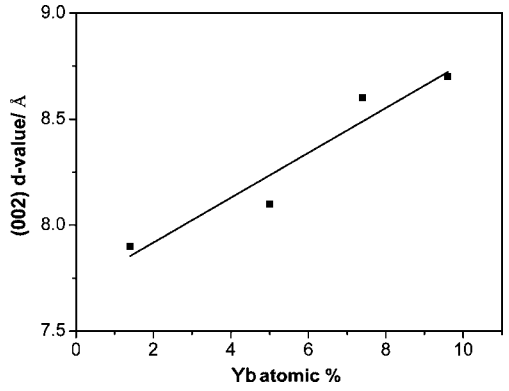

Figure 3. *d*-Spacing values of samples **2a**−**d** as a function of Yb atomic percentage.

content are almost the same for all the samples (see sample compositions reported in Supporting Information, Table SI-2), the displacement of the basal reflections toward higher *d*-spacing values could be seen as a thickening of the sheets due to the insertion of Ln ions, and it could be also interpreted as a clue of the Ln incorporation into the sheet.

Morphological Characterization. A first attempt to study the morphology of the Ln-ZnAl LDH samples was performed by FE-SEM; however, due the nanometric crystal dimensions and their tendency to form aggregates, it was not possible to individuate single particles. Nevertheless, an important information was drawn from elemental mappings of Zn, Al, and Eu in **1a** sample, obtained by a FE-SEM-EDS technique (Supporting Information, Figure SI-2). The local relative concentration of each element present in the sample is indicated by the relative brightness and the intensity of the color. The metals are uniformly distributed throughout the particles of the sample under examination suggesting that the distribution of the Eu(III) ions in the LDH is homogeneous. More detailed information were obtained by TEM images of Ln-ZnAl LDH shown in Figure 4, because of the higher spatial resolution of this technique. Samples containing Europium are constituted by two populations of well formed nanocrystals with quasi-hexagonal shape and different average size (200 and 50 nm) (Figure 4a and 4b). TEM-EDS microanalysis (Supporting Information, Figure SI-3) reveals that the first population is constituted of small crystals of pure ZnAl LDH and the second is constituted of larger crystals of Eu-doped ZnAl LDH, which show higher contrast in TEM imaging

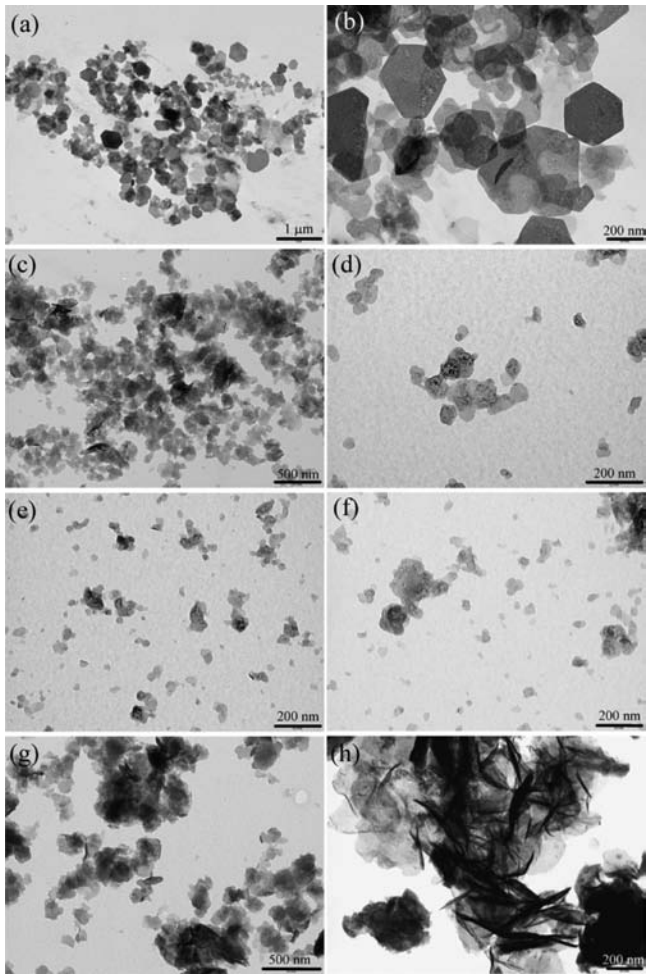

Figure 4. TEM images of samples: **1a** (a) and (b); **3** (c) and (d); **4** (e) and (f) at different magnification and of samples **2a** (g) and **2d** (h).

because of the presence of Eu ions having larger cross sections. These findings suggest that the two nanocrystal populations undergo independent growth processes and the larger dimensions observed for Eu-doped crystals could be due to the necessity to reduce the surface energy (which is determined by the number of unsatisfied bonds).[29] Samples **3** and **4**, containing Nd and Tb respectively, are constituted mainly of a population of platelet with average diameter of 40 nm (Figure

dx.doi.org/10.1021/ic301584g | *Inorg. Chem.* 2012, 51, 13229−13236

4c, d and Figure 4e, f), although it is possible to observe particles with higher average diameter (about 130 nm). Figures 4g and 4h show the TEM images of sample **2a** and **2d** containing 1.4% and 9.6% in Yb, respectively. Two aspects may be highlighted: the samples consist of a single population of particles, with irregular shape (compared to sample **1a**), and the particle size increases with the Yb content from 150 to 400 nm. Moreover, the lamellae of **2d** (Figure 4h) look like "scrolled" at the edge of each crystal. It should be noted that similar scrolled structures have been widely reported for Nb and Ta layered oxides[30,31] and observed with nanosized LDHs referred to as "LDH nanoscrolls".[32] A clearer image of the **2d** sample morphology has been obtained by FE-SEM; in addition FE-SEM images of the **1a**, **3**, **4**, and **2a** samples have been reported (Supporting Information, Figure SI-4).

Thermal Stability. The thermal stability of the Ln-ZnAl LDH samples has been studied by Temperature-dependent X-ray powder diffraction (HT-XRPD), thermogravimetrical (TG) and differential scanning calorimetric (DSC) analyses. Figure 5

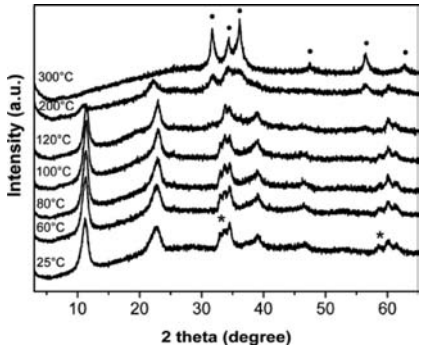

Figure 5. HT-XRPD of sample **1a** at the indicated temperatures. Reflections due to the monoclinic structure (*) and to the ZnO phase (●).

shows the HT-XRPD results related to the sample **1a**. By annealing the sample at temperatures up to 100 °C, the reflections due to the Eu-containing phase are still detectable, suggesting that the structure is maintained. Differently, the treatment at higher temperatures (120 °C) results in the disappearance of reflections due to Eu-containing LDH whereas the overall LDH structure is still retained. The lower thermal stability of Ln-doped nanocrystals compared to the undoped LDH structures suggest an important role of water molecules in the growth of the layer structure. At higher temperatures (300 °C) also the LDH structure is lost and the formation of ZnO occurs. Remarkably, the **1a** sample, imaged after thermal treatment at 120 °C (see Supporting Information, Figure SI-5), shows a morphological change: the undoped small crystals of ZnAl LDH maintain their hexagonal structure (SAED reported in the inset of Supporting Information, Figure SI-5), whereas the larger crystals Eu-ZnAl LDH modify into a rod-shaped amorphous material. Thus, the larger crystals containing Eu are more unstable than the undoped ones because they completely decompose at temperatures higher than 100 °C (see Figures 5 and Supporting Information, Figure SI-5) with the formation of Eu-containing rod-like structures. These data indicate that some structural weakness elements are introduced into the brucitic sheet upon incorporation of Eu(III) ions.

In Figure 6A and 6B the HT-XRPD of **2a** and **2d** samples are reported. Sample **2a** shows the same behavior of the Eu-containing sample **1a**; indeed the reflections due to the low symmetry are detectable till increasing the temperature at 100 °C and disappear for higher temperature treatments, while the LDH peaks are observed up to 200 °C. The samples **3** and **4** showed similar modification of the XRPD pattern upon heating (data not shown). On the other hand, sample **2d** preserves its structure up to 120 °C; over this temperature only the pattern of ZnO is detectable, confirming the presence of a single low-symmetry phase in sample **2d**. To deeply investigate the role of water molecules in Ln(III) doped structures, coupled thermogravimetrical (TG) and differential scanning calorimetric (DSC) studies were performed. Figure 7 shows TG and DSC curves of samples **1c**, **2b**, and **2d** compared with those of ZnAl LDH, and in Table 2 are reported the moles of water lost per mole of sample and the peak temperature at each step. Samples with Ln(III) content lower than 2% showed TG and DSC curves very close to undoped LDH (data not shown); the low lanthanide content did not generate remarkable changes in the weight loss steps. For all the samples in the temperature range 30−300 °C, three different weight losses occur and they are attributable to water molecules differently bonded to the LDH structure.[33] Note that all the thermal processes occurred at lower temperatures with respect of those of ZnAl LDH with high crystallinity very likely due the low crystallinity of the studied samples.[1] In particular, the first weight loss is associated with weakly bound physisorbed water. The following step,

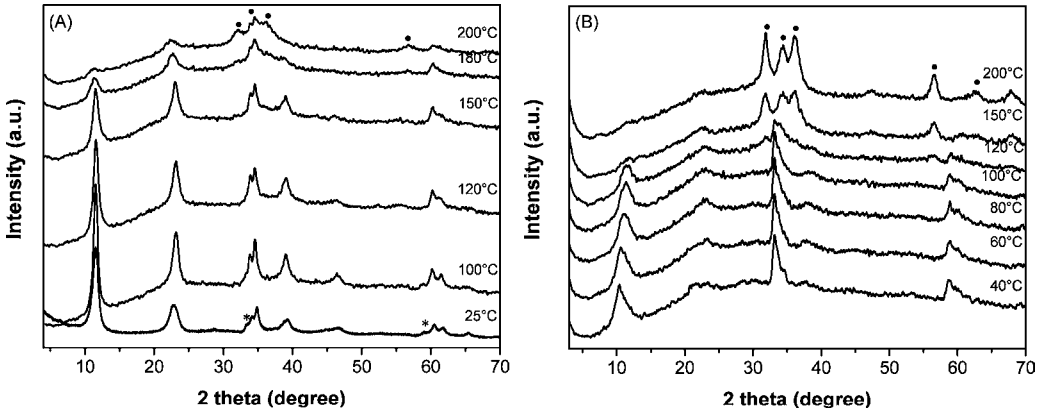

Figure 6. HT-XRPD of **2a** (A) and of **2d** (B) samples at the indicated temperatures. Reflections due to the low symmetry structure (*) and to the ZnO phase (●).

dx.doi.org/10.1021/ic301584g | Inorg. Chem. 2012, 51, 13229−13236

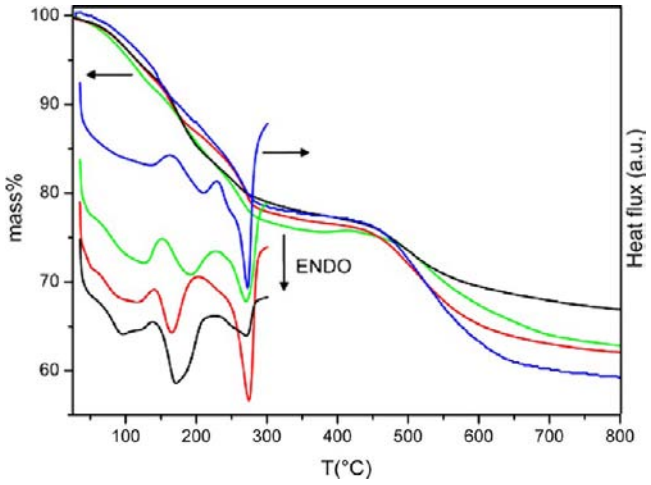

Figure 7. TG and DSC curves of ZnAl LDH (blue), **1c** (green), **2b** (red), and **2d** (black). Operative conditions: air flux, heating rate 10 °C/min.

Table 2. Amount of Water Lost in the Temperature Range 30−300°C of the Indicated Samples[a]

	H_2O (mol/mol LDH) (±0.15%) [peak temperature (°C)]				
sample	1st loss	2nd loss	3rd loss	2rd +3rd	H_2O/Ln molar ratio[b]
ZnAl LDH	0.64 [93]	0.38 [210]	0.45 [272]	0.95	
1c	0.56 [122]	0.52 [190]	0.53 [271]	1.05	1.85
2b	0.52 [93]	0.45 [165]	0.66 [274]	1.11	2.2
2d	0.49 [94]	0.74 [171]	0.43 [270]	1.17	1.8

[a]Molar ratio H_2O/Ln is also reported. [b]H_2O/Ln molar ratio = mol H_2O(2 rd +3rd)-1(constitution water)/mol Ln.

attributed to the loss of interlamellar water and to a partial dehydroxylation of the layer, is strongly affected by the lanthanide content. Indeed, the amount of water lost increases while the peak temperature decreases with the lanthanide loading. It has to be noted that in a conventional LDH, the interlayer water molecules interact directly with interlayer anions and with metal cations through hydrogen bond with OH groups of the brucitic sheets; thus the dehydration process is mainly determined by the nature of both the interlayer anions and the layer cations.[1] All the materials under investigation contain bromide as counterion that can interact with the water molecules via ion-dipole interaction. Consequently, the difference observed in the thermal behavior of the samples (Table 2) are due to the lanthanide ions that can coordinate water molecules to fill their coordination vacancies. The loss of the coordinated water,[34] occurring at temperatures lower than those of interlayer hydrogen bonded water (210 °C), results into Ln ions with unsaturated coordination spheres. To recover the coordination sphere of the Ln ions the brucite sheet could be forced to close onto itself to form the scrolled materials. Moreover, the scrolled morphology induces an early dehydroxylation of the sheets that causes the destruction of the Ln-containing LDH structure, as shown by HT-XRPD (Figure 5 and 6). Finally, the third weight loss at about 270 °C is associated to the complete dehydroxylation of the layers. This peak temperature seems to be independent of the metal nature. Assuming that the water lost in the second and third step is the sum of the interlayer and constitution water (1 mol of constitution water per mole of LDH) it is possible to determine the interlayer water. This value is higher in the presence of Ln(III) in the structure thus confirming the role of water molecules to full-fill the coordination sphere of the Ln cations and accounting for the lower stability of the materials. At this stage the effect of Ln(III) content on the amount of interlayer water cannot be drawn although DSC data show that the molar ratio between the interlayer water and the lanthanide ion is close to a value of two (Table 2). For the sample **2d**, for which the data suggest it to be constituted by a pure phase, the following minimal formula: $[Zn_{0.795}Al_{0.109}Yb_{0.096}(OH)_2]$-$Br_{0.205}$0.66 H_2O has been determined by means of ion chromatography, ICP, elemental analysis, and TG data. On the basis of previous discussion the 0.66 mols of water include both physisorbed and coordinated water.

Spectroscopic Characterization. To gain more insights into the structural properties of Ln containing samples infrared spectroscopy has been employed. Infrared spectra measured in the 400−1100 cm^{-1} frequency range of **2b**, **2d**, and **2e** samples (5.0, 9.6, 17.0% of Yb, respectively) are shown in Figure 8A together with the spectrum of pure ZnAl LDH. The overall spectral profile obtained for the undoped ZnAl LDH reminds one of that reported for other LDH and is commonly associated to lattice vibrations of OHs groups.[35−40] Specifically, the broad signal at around 605 cm^{-1} and the band at about 430 cm^{-1} can be generically related to metal−OHs vibration modes.[35,37−39] In a recent study a very similar spectrum has been reported for a MgAl LDH sample and a more specific assignment of the components proposed.[38] In particular, the

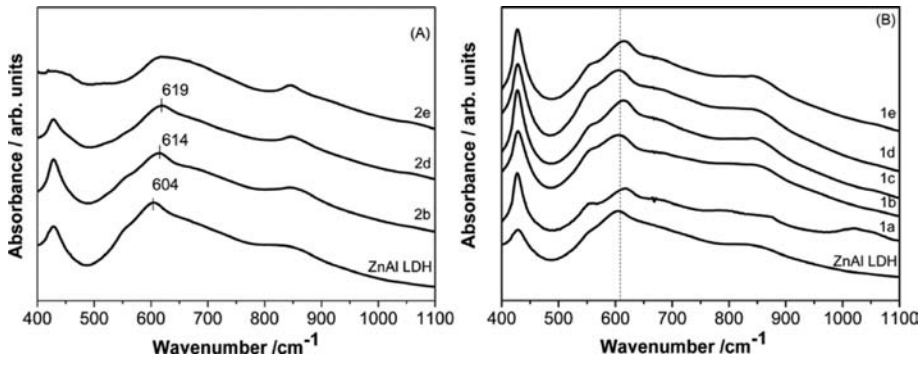

Figure 8. Infrared spectra of pure ZnAl LDH and of Yb doped samples **2b**, **2d**, and **2e** (A) and of Eu-doped samples **1a−e** (B).

dx.doi.org/10.1021/ic301584g | Inorg. Chem. 2012, 51, 13229−13236

broad distribution around 605 cm^{-1} has been attributed to OH rotations (MOH bending) while the band at about 450 cm^{-1} to OH translations (MOM bending/stretching); this latter signal is considered indicative of lattice ordering.[40] As it can be seen in Figure 8A, the increase of the Yb content from 0 to 9.6% only leads to minor spectral variations suggesting that the incorporation of the lanthanide is not accompanied by a strong reorganization of the brucitic sheet. Nevertheless, the systematic upshift of the 605 cm^{-1} component and the broadening of the ~430 cm^{-1} band observed at higher Yb concentrations seem consistent with the progressive structural variation resulting from XRPD data. These findings may also reflect the occurrence of Ln-induced small modulations of metal−OHs interactions. On the other hand, increasing the Yb fraction to 17.6% (sample **2e**) corresponds to more evident spectral variations, in line with the occurrence of the ZnO segregation detected by diffraction data. Infrared spectra of Eu-ZnAl LDH samples are reported in Figure 8B. In this case the main spectral features are maintained at all concentrations and only small and unsystematic frequency shifts of the 605 cm^{-1} component are observed. This is probably not surprising considering the nonspecific character of the signals in the depicted spectral region and the relatively small fractions of Eu incorporated in these samples. The presence of the intense peak at 430 cm^{-1} points out the preservation of lattice ordering at all lanthanide fractions considered.[40]

It is well established that the luminescence properties of Ln(III) are strongly dependent on the environment. In the present work luminescent measurements were carried out to investigate whether the inclusion in the LDH layer structure affects the electronic properties of lanthanide ions. Luminescence measurements were concentrated on Eu(III) and Tb(III) samples, because of the spectral sensitivity of the instrument at disposal. The luminescence properties of Eu- and Tb-ZnAl LDH samples were investigated by steady-state techniques upon direct excitation of Ln(III) in the solid samples. As previously reported[18,20,25] the photoluminescence spectra could be easily detected at room temperature upon excitation into the $^7F_0$-$^5L_6$ transition of Eu(III) at 393 nm and into the $^7F_6$-$^5G_6$ transition of Tb(III) at 375 nm, and they are shown in Figure 9 for the samples **1a, b, d** and **4**. The emission spectra (Figure 9) can be assigned to the typical $^5D_0$-^7F_J (J = 1, 2, 3, 4) transitions of Eu(III) ion and $^5D_4$-^7F_J (J = 1, 2, 3) transitions of Tb(III). In Figure 9 the photoluminescence excitation spectra are also reported which consist in a series of bands ascribed to intra-$4f^6$ transitions of the Ln ions; the band broadening clearly observed in all samples and particularly evident for sample **1a** can account for the effect of LDH matrix in energy level positions. In general the emission spectra are dominated by the electric-dipole transitions indicating that the Ln(III) ions experience a low symmetry crystal field in the materials, supporting the hypothesis that the lanthanide ions have been included in the LDH lamellae. However, at different Eu(III) loadings, the intensity ratios between the peak at 595 ($^5D_0$-$^7F_1$) and 615 ($^5D_0$-$^7F_2$) nm change; this behavior can be related to modification of the crystal field upon increasing the Eu(III) loading since the $^5D_0$-$^7F_1$, which is a magnetic-dipole transition, is thus not influenced by the chemical environment of the ions, while the $^5D_0$-$^7F_2$ transition is strongly affected by the field symmetry. The continuous decrease of the 615 nm intensity with the increase of Eu loading is likely due to a structural modification of the materials in agreement with XRPD results. This hypothesis is further confirmed by the peak ratio determined for the sample **1a** after thermal treatment. These data indicate that the inclusion of Ln(III) ions in a brucitic layer does not alter their electronic configurations; however, the symmetry of the inclusion site can modulate the spectral brightness of the prepared materials.

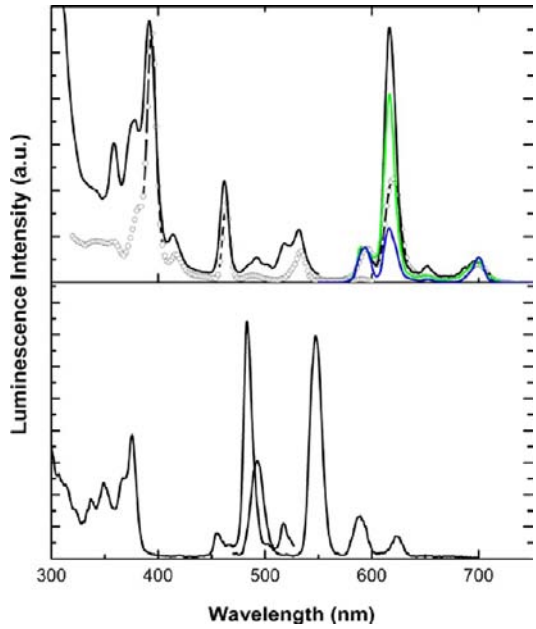

Figure 9. Emission and excitation spectra of samples **1a** (black line), **1b** (green line), **1d** (blue line), **1a** after thermal treatment (circles), and **4** (black line, lower panel). Excitation at 393 and 375 nm for Eu(III) and Tb(III) samples, respectively.

CONCLUSIONS

The incorporation of Ln(III) cations having different ionic radius into the LDH lamellae has been achieved by preparing the crystals in a confined environment. Differently from the conventional synthetic methods, the water pools of the inverse micellae acted as a microreactor where materials with unexpected characteristics and properties were obtained. The effects of lanthanide loading on the structure, morphology, and thermal behavior of the layered nanocrystals were investigated. The different techniques and methods used in the present work indicate that the Ln(III)-doping is a complex process involving several factors. Structural information were obtained by XRPD which showed, upon Ln(III) inclusion into the brucitic sheets, the formation of a low symmetry phase with monoclinic structure. The amount of the lanthanide ions included into the brucitic sheet is affected by the Ln(III) ionic radius: the large Eu(III) can be inserted into the LDH structure in average atomic percentages lower than 2.7%, in which the lanthanide occupies sites not having inversion center, as established by steady state luminescence measurements; the small Yb(III) can be incorporated into the layer structure up to about 10%, leading to progressive phase transformation of the pristine LDH structure to pure monoclinic phase. The nature and the amount of Ln(III) in the LDH determine the morphology of the nanoparticles that exhibit dimension ranging from 50 to 400 nm. Moreover, thermogravimetrical (TG) and differential scanning calorimetric (DSC) studies indicate that Ln-doped LDH possess a lower thermal stability compared to the undoped ones suggesting the crucial role of water molecules that are essential to satisfy coordination sphere of incorporated

dx.doi.org/10.1021/ic301584g | Inorg. Chem. 2012, 51, 13229−13236

Ln cations. IR spectra on Yb- and Eu-doped samples support the incorporation of Ln(III) into the LDH lamellae. Spectral variations observed at increasing Yb concentrations are broadly consistent with structural changes resulting from XRPD measurements. The obtained materials deserve a further characterization especially as regards the intercalation and ion exchange properties compared to those of undoped LDH and the matrix effects on the luminescence properties.

■ ASSOCIATED CONTENT

Supporting Information

Amounts of salts used in the preparations, composition of the Ln-ZnAl samples, LeBail plots of: crystalline ZnAl-LDH in bromide form, **2a** and **2d** samples, FE-SEM and EDS images and TEM-EDS of **1a** sample, FE-SEM image of **1a**, **3**, **4**, **2a** and **2d** sample. This material is available free of charge via the Internet at http://pubs.acs.org.

■ AUTHOR INFORMATION

Corresponding Author

*Fax: +390755855566. Phone: +390755855563. E-mail: nocchett@unipg.it.

Present Address

[†]Laboratory MIST E-R and Consiglio Nazionale delle Ricerche, Istituto per lo Studio dei Materiali Nanostrutturati (CNR-ISMN), Via P. Gobetti 101, I-40129 Bologna, Italy.

Notes

The authors declare no competing financial interest.

■ ACKNOWLEDGMENTS

This work was supported by the Università di Perugia and the Ministero per l'Università e la Ricerca Scientifica e Tecnologica (Rome), MIUR–Project FIRB 2010 No. RBFR10CWDA_003.

■ REFERENCES

(1) Rives, V., Ed.; *Layered Double Hydroxides: Present and Future*; Nova Science Publishers: New York, 2001.

(2) Leroux, F.; Taviot-Guého, C. *J. Mater. Chem.* **2005**, *15*, 3628.

(3) Evans, D. G.; Duan, X. *Chem. Commun.* **2006**, *5*, 485.

(4) Del Hoyo, C. *Appl. Clay Sci.* **2007**, *36*, 103.

(5) Choy, J. H.; Oh, J. M.; Biswick, T. T. *J. Mater. Chem.* **2009**, *19*, 2553.

(6) (a) Tammaro, L.; Costantino, U.; Nocchetti, M.; Vittoria, V. *Appl. Clay Sci.* **2009**, *43*, 350. (b) Costantino, U.; Bugatti, V.; Gorrasi, G.; Montanari, F.; Nocchetti, M.; Tammaro, L.; Vittoria, V. *ACS Appl. Mater. Interfaces* **2009**, *1*, 668. (c) Costantino, U.; Montanari, F.; Nocchetti, M.; Canepa, F.; Frache, A. *J. Mater. Chem.* **2007**, *17*, 1079. (d) Aloisi, G. G.; Elisei, F.; Nocchetti, M.; Camino, G.; Frache, A.; Costantino, U.; Latterini, L. *Mater. Chem. Phys.* **2010**, *123*, 372.

(7) (a) Choy, J. H.; Kwak, S. Y.; Jeong, Y. J.; Park, J. S. *Angew. Chem., Int. Ed.* **2000**, *39*, 4041. (b) Bellezza, F.; Cipiciani, A.; Latterini, L.; Posati, T.; Sassi, P. *Langmuir* **2009**, *25*, 10918. (c) Perioli, L.; Posati, T.; Nocchetti, M.; Bellezza, F.; Costantino, U.; Cipiciani, A. *Appl. Clay Sci.* **2011**, *53*, 374. (d) Costantino, U.; Ambrogi, V.; Nocchetti, M.; Perioli, L. *Microporous Mesoporous Mater.* **2008**, *107*, 149. (e) Ricci, M.; Schoubben, A.; Rossi, A.; Blasi, P.; Latterini, L.; Aloisi, G. G.; Rossi, C.; Perioli, L. *Int. J. Pharm.* **2005**, *295*, 47. (f) Bertini, B.; Nocchetti, M.; Ricci, M.; Ambrogi, V.; Rossi, C.; Perioli, L.; Latterini, L. *Eur. J. Pharm. Sci.* **2006**, *62*, 185. (g) Ambrogi, V.; Ciarnelli, V.; Nocchetti, M.; Perioli, L.; Rossi, C. *Eur. J. Pharm. Sci.* **2009**, *73*, 285. (h) Posati, T.; Bellezza, F.; Tarpani, L.; Perni, S.; Latterini, L.; Marsili, M.; Cipiciani, A. *Appl. Clay Sci.* **2012**, *55*, 62.

(8) (a) Turco, M.; Bagnasco, G.; Costantino, U.; Marmottini, F.; Montanari, T.; Ramis, G.; Busca, G. *J. Catal.* **2004**, *228*, 43. (b) Montanari, T.; Sisani, M.; Nocchetti, M.; Vivani, R.; Delgado, M. C. H.; Ramis, G.; Busca, G.; Costantino, U. *Catal. Today* **2010**, *152*, 104.

(9) Latterini, L.; Nocchetti, M.; Aloisi, G. G.; Costantino, U.; De Schryver, F.; Elisei, F. *Langmuir* **2007**, *23*, 12337.

(10) Costantino, U.; Nocchetti, M.; Sisani, M.; Vivani, R. *Z. Kristallogr.* **2009**, *224*, 273.

(11) Mousty, C.; Kaftan, O.; Prevot, V.; Forano, C. *Sens. Actuators, B* **2008**, *133*, 442.

(12) Li, C.; Wang, G.; Evans, D. G.; Duan, X. *J. Solid State Chem.* **2004**, *177*, 4569.

(13) Chang, Z.; Evans, D.; Duan, X.; Boutinaud, P.; de Roy, M.; Forano., C. *J. Phys. Chem. Solids* **2006**, *67*, 1054.

(14) (a) Bastianini, M.; Costenaro, D.; Bisio, C.; Marchese, L.; Costantino, U.; Vivani, R.; Nocchetti, M. *Inorg. Chem.* **2012**, *51*, 2560. (b) Ma, R.; Liang, J.; Takada, K.; Sasaki, T. *J. Am. Chem. Soc.* **2011**, *133*, 613.

(15) Stumpf, T.; Curtius, H.; Walther, C.; Daedenne, K.; Ufer, K.; Fanghanel, T. *Environ. Sci. Technol.* **2007**, *41*, 3186.

(16) Chen, Y.; Zhou, S.; Li, F.; Wei, J.; Dai, Y.; Chen, Y. *J. Fluoresc.* **2011**, *21*, 1677.

(17) Gao, X.; Lei, L.; Lu, C.; Sun, Y.; Zheng, H.; Cui, Y. *J. Solid State Chem.* **2008**, *18*, 11776.

(18) Gunawan, P.; Xu, R. *J. Phys. Chem. C* **2009**, *113*, 17206.

(19) Chen, H.; Zhang, W. *J. Am. Ceram. Soc.* **2010**, *93*, 2305.

(20) Wang, J.; Zhou, J.; Li, Z.; Song, Y.; Liu, Q.; Jiang, Z.; Zhang, M. *Chem.—Eur. J.* **2010**, *16*, 14404.

(21) Musumeci, A. W.; Xu, Z. P.; Smith, S. V.; Minchin, R. F.; Martin, D. J. *J. Nanopart. Res.* **2010**, *12*, 111.

(22) Gao, X.; Hu, M.; Lei, L.; O'Hare, D.; Markland, C.; Sun, Y.; Faulkner, S. *Chem. Commun.* **2011**, *47*, 2104.

(23) Chen, Y.; Li, F.; Zhou, S.; Wei, J.; Dai, Y.; Chen, Y. *J. Solid State Chem.* **2010**, *183*, 2222.

(24) Zhao, Y.; Li, J. G.; Fang, F.; Chu, N.; Ma, H.; Yang, X. *Dalton Trans.* **2012**, *41*, 12175.

(25) Posati, T.; Bellezza, F.; Cipiciani, A.; Costantino, F.; Nocchetti, M.; Tarpani, L.; Latterini, L. *Cryst. Growth Des.* **2010**, *10*, 2847.

(26) Bellezza, F.; Cipiciani, A.; Costantino, U.; Nocchetti, M.; Posati, T. *Eur. J. Inorg. Chem.* **2009**, 2603.

(27) Bellezza, F.; Nocchetti, M.; Posati, T.; Giovagnoli, S.; Cipiciani, A. *J. Colloid Interface Sci.* **2012**, *376*, 20.

(28) Le Bail, A. *Powder Diffr.* **2005**, *20*, 316.

(29) Cao, G. *Nanostructure and Nanomaterials*; Imperial College Press: London, U.K., 2004; and references therein.

(30) Kobayashi, Y.; Hata, H.; Salama, M.; Mallouk, T. E. *Nano Lett.* **2007**, *7*, 2142.

(31) Eguchi, M.; Angelone, M. S.; Yennawar, H. P.; Mallouk, T. E. *J. Phys. Chem. C* **2008**, *112*, 11280.

(32) Ren, L.; Hu, J. S.; Wan, L. J.; Bai, C. L. *Mater. Res. Bull.* **2007**, *42*, 571.

(33) Frost, R. L.; Martens, W.; Ding, Z.; Kloprogge, J. T. *J. Therm. Anal. Calorim.* **2003**, *71*, 429.

(34) Masuda, Y.; Nagaoka, K.; Ogawa, H.; Nakazato, O.; Yukawa, Y.; Miyamoto, H. *J. Alloys Compd.* **1996**, *235*, 23.

(35) Fernández, J. M.; Ulibarri, M. A.; Labajos, F. M.; Rives, V. *J. Mater. Chem.* **1998**, *8*, 2507.

(36) Kloprogge, J. T.; Frost, R. L. *J. Solid State Chem.* **1999**, *146*, 506.

(37) Hickey, L.; Kloprogge, J. T.; Frost, R. L. *J. Mater. Sci.* **2000**, *35*, 4347.

(38) Pérez-Ramírez, J.; Mul, G.; Moulijn, J. A. *Vib. Spectrosc.* **2001**, *27*, 75.

(39) Kloprogge, J. T.; Hickey, L.; Frost, R. L. *J. Solid State Chem.* **2004**, *177*, 4047.

(40) Richardson, M. C.; Braterman, P. S. *J. Phys. Chem. C* **2007**, *111*, 4209.